ELSEVIER

Polymer 40 (1999) 1019–1023

polymer

Preparation and microphase-separated structures of $(AB)_n$ star–block copolymers composed of symmetric diblock arms

Satoshi Uchida*, Ayako Ichimura, Koji Ishizu

Department of Polymer Science, Tokyo Institute of Technology, 2-12 Ookayama, Meguro-ku, Tokyo 152, Japan

Received 19 December 1997; accepted 20 April 1998

Abstract

The $(AB)_n$ star copolymers (arm number $n = 7–77$; polyisoprene blocks = *ca*. 50 vol%) were synthesized by copolymerization of polystyrene (PS)–*block*–polyisoprene (PI) diblock anions with divinylbenzene (DVB) in benzene. The arm numbers were controlled by changing the initial concentration of the diblock anion or the feed ratio of DVB to the diblock anion end. The microphase-separated structures of $(AB)_n$ star copolymers were studied by means of transmission electron microscopy (TEM) and small-angle X-ray scattering (SAXS). It was found that the $(AB)_n$ star copolymers composed of symmetric arms ($n < 77$) formed lamellar structures. The periodic distances of $(AB)_n$ star copolymers ($n < 77$) were the same as those of the corresponding diblock arms.

Keywords: $(AB)_n$ star–block copoymer; Microphase-separated structure; Domain spacing

1. Introduction

The microdomain morphology of a particular copolymer is determined by the minimization of the free energy of the system. In the classical picture, the phase behaviour of linear diblock copolymers depends on only two parameters: the composition (f) and the reduced interaction parameter (χN), where N is the total number of the segments [1]. Investigation of $(AB)_n$ star copolymers found, in addition to the three classical microdomain morphologies of lamellae, cylinders and spheres, a new morphology such as tetrapod type [2–9]. It was found that the [polystyrene (PS)–*block*–polyisoprene (PI)]$_n$ $(SI)_n$ stars ($n = 4$ and 12; PS volume fraction of ca. 0.5) formed lamellar structures and their lamellar periodic distances were essentially the same as those of the arm molecules, that is, linear diblock copolymers, irrespective the number of arms [9].

In previous works [10–12], we prepared the $(SI)_n$ star copolymers (PI block, ca. 19 wt%) by copolymerization of PS–*block*–PI diblock anions with DVB. It was found from the small-angle X-ray scattering (SAXS) and transmission electron microscopy (TEM) measurements that these stars (arm number $n > 15$) led to hierarchical transformation of cubic lattices. That is to say, the $(SI)_n$ stars were packed with a lattice of body-centred cubic (BCC) structure near the overlap threshold (C^*). This structure changed to a mixed lattice of BBC and a face-centred cubic (FCC) with increasing polymer concentration. Near the bulk film, these mixed structures changed to a lattice of FCC. Such a transformation could be explained by the thermal blob model for a star polymer proposed by Daoud and Cotton [13]. According to theoretical results, the central cores of star polymers do not interpenetrate with each other even beyond the C^*. Then, the $(SI)_n$ stars form a unimolecular micelle in solution and lead to hierarchical structural ordering. However, it is an unclarified problem whether such hierarchical transformations of lattice appear or not, even in the $(SI)_n$ stars composed of symmetric diblock arms.

In this article, we prepared the $(SI)_n$ stars composed of symmetric diblock arms by copolymerization of PS–*block*–PI diblock anions with DVB. Microphase separation of such star block copolymers was investigated by means of SAXS and TEM measurements as a parameter of arm number.

2. Experimental

2.1. Synthesis and characterization of $(AB)_n$ stars

$(AB)_n$ star copolymers were prepared by copolymerization of PS–*block*–PI diblock anions with DVB (Merch; 65%, *m*-/*p*-isomer = 2; 35%, ethylstyrene) initiated

* Corresponding author.

PII S0032-3861(98)00315-2

Table 1
Experimental conditions and characteristics of $(SI)_n$ stars[a]

Code	PS–*block*–PI arm			$(AB)_n$ star					
	$10^{-4}\bar{M}_n$[b]	$\bar{M}_w/\bar{M}_n$[c]	PI (vol%)[d]	[LE] (mol l^{-1})	[DVB]/[LE] (mol mol^{-1})	Yield (%)[c]	$10^{-6}\bar{M}_w$[e]	$\bar{M}_w/\bar{M}_n$[c]	n[f]
$(SI44)_{25}$	4.37	1.10	46.6	2.73	4.4	51.3	1.09	1.03	25
$(SI44)_{43}$				2.78	9.4	62.6	1.88	1.06	43
$(SI61)_7$	6.14	1.03	52.7	1.10	2.8	22.8	0.41	1.04	6
$(SI61)_{16}$				0.93	3.8	44.6	0.98	1.02	16
$(SI61)_{26}$				2.91	3.4	45.5	1.62	1.03	26
$(SI61)_{77}$				6.29	3.2	27.0	4.73	1.04	77

[a] Copolymerized in benzene at 60°C for 24 h.
[b] Calculated from the Mn of PS precursor and the molar fraction of styrene.
[c] Determined by g.p.c. (relative to polystyrene homopolymer).
[d] Determined by ^{1}H-n.m.r. in $CDCl_3$.
[e] Determined by g.p.c. equipped with low-angle laser-scattering detector.
[f] Arm number per macromolecule.

by *n*-butyllithium (*n*-BuLi) in benzene. This solution was stirred at 20°C for 24 h and the temperature was subsequently raised to 50°C. The star copolymers were fractionated in a benzene–methanol mixture in order to remove the unreacted arm materials. The details of the synthetic procedure and characterization were given elsewhere [10,11]. The microstructure of PI blocks from this method contained 12% 1,2-, 43% 3,4-, and 45% 1,4-structures by ^{1}H nuclear magnetic resonance (n.m.r.) spectroscopy.

2.2. Morphological observation

The films of $(AB)_n$ star copolymer and diblock arm polymer were cast from 5 wt% of benzene solutions. The solvent was evaporated as slowly as possible (more than a week). Then the films were annealed at 110°C for 5–7 days under vacuum to form the equilibrium structure. In these annealing conditions, the $(SI)_n$ stars did not degradate during such an annealing process, because gel permeation chromatography (g.p.c.) profiles after annealing treatments showed the same elution pattern as those of original stars. The films were cut perpendicular to the film surface with a thickness of 100 nm by microtome (Reichert-Nissei ULTRACUT N). The thin film sections were picked up on a copper grid and exposed to osmium tetroxide (OsO_4) vapour for 24 h. Morphological results were obtained on a Hitachi H-500 TEM at 75 kV.

2.3. SAXS measurement

The SAXS intensity distribution was measured with a rotating-anode X-ray generator (Rigaku Denki Rotaflex RTP 300RC) operated at 40 kV and 100 mA. The X-ray source was monochromatized to Cu K_α ($\lambda = 1.5418$ Å) radiation. The SAXS patterns were taken with a fine-focused X-ray source using a flat plate camera (Rigaku Denki, RU-100). The SAXS intensity profiles were plotted from the horizontal section of the SAXS patterns without considering the smearing correction.

3. Results and discussion

3.1. Synthesis of $(AB)_n$ stars

As mentioned in the introduction, we synthesized $(AB)_n$ stars by free radical microgelation in micelles formed by copolymerization PS–*block*–PI diblock macromonomers [14,15] (PI block = 19–50 wt%) with DVB or copolymerization of diblock monoanions with DVB [11] (PI block = 19 wt%). This synthetic method is the most convenient way to control the high number of arms. It is interesting to apply this method for the synthesis of $(AB)_n$ stars with symmetric arms. We prepared $(SI)_n$ stars with various arm numbers, by varying the initial concentration of PS–*block*–PI monoanions ([LE]) and the concentration ratio of DVB to PS–*block*–PI monoanions ([LE]/[DVB]). Table 1 lists the experimental conditions and results for $(AB)_n$ star formation. The number-average molecular weight (M_n) of the SI arm was determined by universal calibration [16] ($\log[\eta]M$ versus elution volume) by g.p.c. These observed values were in good agreement with the M_n calculated from the M_n of the PS precursor and the composition of the PS block. The weight-average molecular weight (M_w) of $(SI)_n$ star was determined not only by static light scattering but also by g.p.c. equipped with low-angle laser-light scattering detector [17]. The refractive increment d*n*/d*c* was determined by the differential refractometer for each star arm precursor.

A typical g.p.c. profile of $(SI44)_{25}$ is shown in Fig. 1. The g.p.c. distribution is bimodal according to the refractive index (r.i.) monitor but unimodal according to the ultraviolet (u.v.) monitor. The wavelength of u.v. is set at 292 nm, i.e. at the characteristic absorption of vinylbenzyl groups of DVB. In the r.i. chart, the low molecular weight

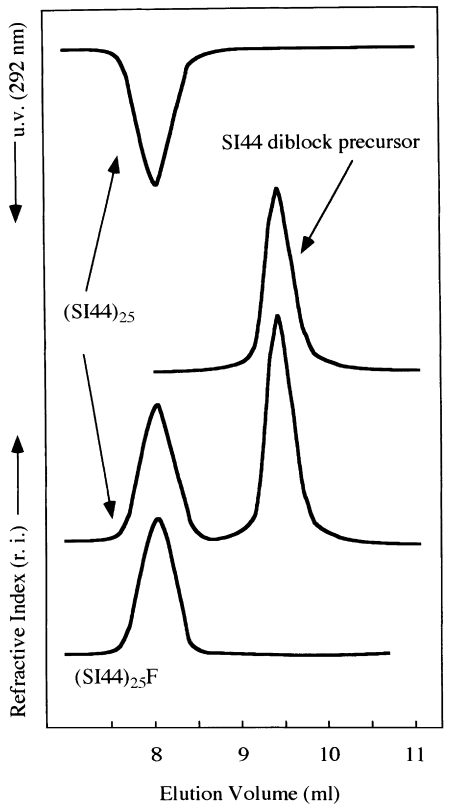

Fig. 1. G.p.c. profiles of $(SI44)_{25}$ star and SI44 diblock copolymers.

fraction was agreement with the elution pattern of the SI diblock precursor. Therefore, the copolymerization product is a mixture of $(SI)_n$ star and its precursor. In the u.v. chart, unreacted SI precursor has no adsorption at 292 nm. This indicates that all of the feed DVB are consumed in the core formation of the star copolymers. Moreover, macrogelation was not observed in any of the experiments during copolymerization. Polymerization yields are in the range of 23–63%. The polymerization mechanism can be speculated from these results as follows. The PS–*block*–PI monoanion is added rapidly to DVB. Therefore, part of the feed diblock anions would form linear PS–*block*–PI macromonomer anions possessing terminal pendant double bonds at the initial stage of the reaction. These macromonomers would form uniform micelle even in a good solvent. It is found from previous works [14,18] that symmetric diblock copolymers formed mesomorphic structure such as a wormlike micelle in a good solvent at high polymer concentration. As a result, core formation by crosslinking may proceed within such micelles. In these copolymerization systems, the residual PS–*block*–PI anions unadded to DVB cannot penetrate into DVB core of $(AB)_n$ stars due to high segment density. In Table 1, the code number, for example, $(SI44)_{25}$ represents the SI star with arm number $n = 25$ and arm molecular weight $M_n = 4.4 \times 10^4$. The arm number of the $(SI)_n$ stars increased not only with increasing [DVB]/[LE] but also with increasing the initial concentration [LE] of PS–*block*–PI anions. Each $(SI)_n$ star was

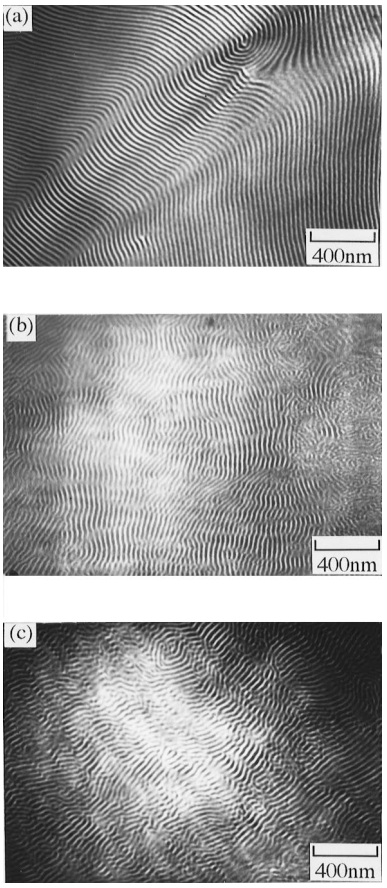

Fig. 2. TEM micrographs of diblock arm and $(SI44)_n$ star films stained with OsO_4: (a) SI44 diblock arm; (b) $(SI44)_{24}$ star; (c) $(SI44)_{43}$ star.

removed from the corresponding unreacted SI diblock precursor by the precipitation fractionation (benzene–methanol system). So, the $(SI)_n$ star fraction denotes as $(SI)_nF$ in following discussion. G.p.c. profile of $(SI45)_{25}F$ is also shown in Fig. 1. The g.p.c. distribution is unimodal. This star had apparently a narrow molecular weight distribution ($M_w/M_n = 1.02$). The absolute M_n of the $(SI)_n$ stars could not be determined by means of osmometry, because their molecular weights were too high. It should be noticed that the M_w/M_n determined by g.p.c. is overestimated as compared with the absolute values due to highly branched structures. Moreover, the $(SI)_nF$ stars obtained in this work seem to have low polydispersity due to the copolymerization system of uniform micelles.

3.2. Microphase-separated structure of $(SI)_n$ star

We studied the behaviour of the microphase-separated structure of $(SI)_n$ stars with symmetric arms as a parameter of the number of arms. Fig. 2 shows TEM micrographs of SI44 diblock arm and $(SI44)_nF$ star in the bulk film. The dark portions correspond to PI phases selectively stained with OsO_4. All of these specimens show alternating PS/PI lamellar morphology. The periodic distances of lamellae for these specimens seem to be equal.

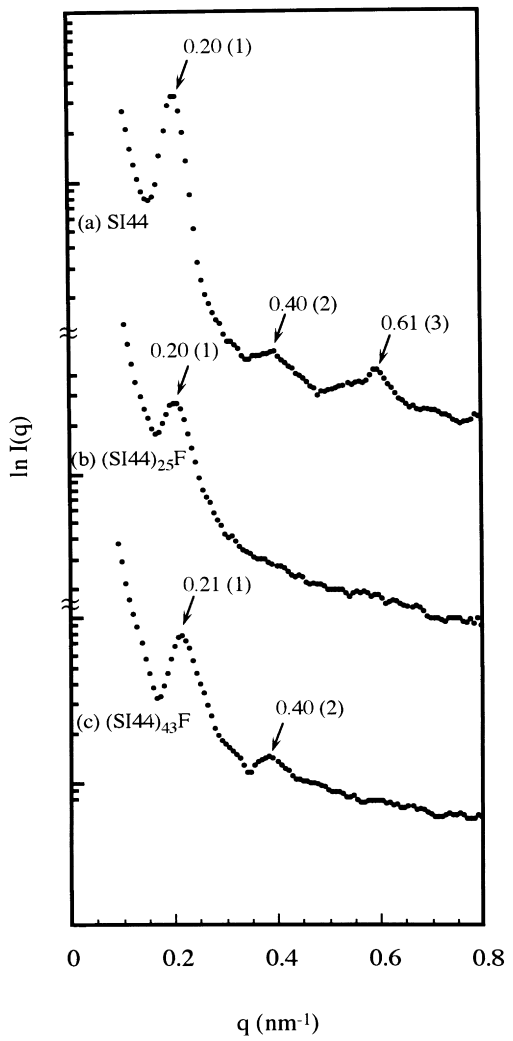

Fig. 3. SAXS intensity profiles of diblock arm and $(SI44)_n$ star films: (a) SI44 diblock; (b) $(SI44)_{24}$ star; (c) $(SI44)_{43}$ star.

In order to estimate accurate domain spacings, we therefore performed the SAXS measurements for these samples. Fig. 3a shows the SAXS intensity profile of the SI44 diblock arm film at the edge view, where $q[= (4\pi/\lambda)\sin\theta]$ is the magnitude of the scattering vector. The arrows show the scattering maxima and the values indicate the scattering vectors. On the other hand, the values in the parentheses indicate the interplaner spacings (d_l/d_i) calculated from Bragg reflections. The first three strong diffraction peaks are observed at the relative q positions of 1 : 2 : 3 as shown by arrows. The interplaner spacing at the scattering angles is relative to the angle of the first maximum according to Bragg equation : $2d \sin\theta = \lambda$ (where θ is one-half of the scattering angle, $\lambda = 1.5418$ Å). This packing pattern corresponds to lamellar morphology. For the $(SI44)_{25}F$ and $(SI44)_{43}F$ star films (Fig. 3b,c), the first peak only and first two peaks, respectively, appear in the SAXS profiles but these peaks show almost the same position as that obtained in SI44 diblock arm. Table 2 summarizes the domain spacings of SI44 diblock arm and $(SI44)_nF$ stars ($n = 25$ and 43) calculated from SAXS and TEM measurements. It is found that both experimental values (D) are almost equal within experimental errors. Moreover, it is also found that the periodic distances of $(SI44)_nF$ star ($n = 25$ and 43) are well in agreement with that of lamellar microdomain for SI44 diblock arm. These results are similar to those reported by Matsushita et al. [9].

Table 2
Domain spacings of SI55 diblock arm and $(SI44)_n$ stars

Code	q_1 (nm^{-1})	Periodic distance: D (nm)	
		From SAXS	From TEM
SI44	0.201	31.2	30.8
$(SI44)_{25}F$	0.204	30.8	30.5
$(SI44)_{43}F$	0.211	29.8	29.8

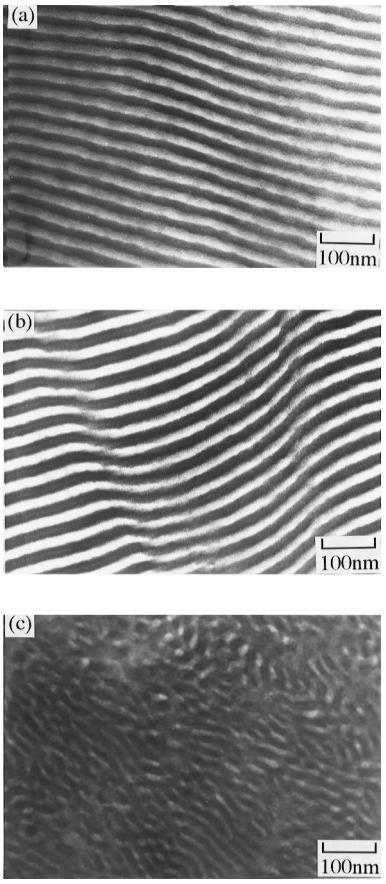

Fig. 4. TEM micrographs of diblock arm and $(SI61)_n$ star films; (a) SI61 diblock arm; (b) $(SI61)_{26}$ star; (c) $(SI61)_{77}$ star.

It is interesting how the behaviour of the microphase-separated structure show the $(SI)_n$ stars with extremely high arms. Then, we studied the microphase separation of $(SI61)_nF$ stars ($n = 26$ and 77) in the bulk. Both SI61 and $(SI61)_{26}F$ films show alternating PS/PI lamellar morphology and have almost the same periodic distance (Fig. 4a,b). However, it is remarkable from the TEM image that $(SI61)_{77}$ star shows lamellar-like morphology but has a

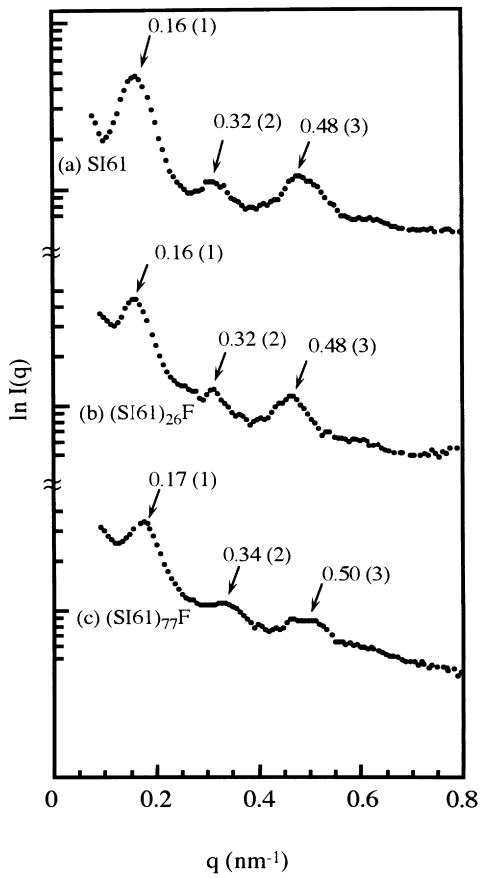

Fig. 5. SAXS intensity profiles of diblock arm and $(SI61)_n$ star films: (a) SI61 diblock arm; (b) $(SI61)_{26}$ star; (c) $(SI61)_{77}$ star.

Table 3
Domain spacings of SI61 diblock arm and $(SI61)_n$ stars

Code	q_1 (nm^{-1})	Periodic distance: D (nm)	
		From SAXS	From TEM
SI61	0.162	38.8	39.0
$(SI61)_7F$	0.161	39.0	39.4
$(SI61)_{16}F$	0.162	38.8	40.0
$(SI61)_{26}F$	0.162	38.8	39.3
$(SI61)_{77}$	0.172	36.5	31.5

smaller periodic distance compared to those obtained for other specimens. It is also noticeable that these lamellar structures have some kind of curvature.

Fig. 5 shows typical SAXS intensity profiles of SI61 diblock arm and $(SI61)_nF$ star films ($n = 26$ and 77) at the edge view. In SI61 and $(SI61)_{26}F$ films (Fig. 5a,b), the first three scattering peaks appear at the relative q positions of 1 : 2 : 3 as shown by arrows. These packing patterns correspond to lamellar structure. The first q_1 values are almost the same for both films. The similar result was obtained for the $(SI61)_7F$ and $(SI61)_{16}F$ star films.

The $(SI61)_{77}F$ film shows lamellar packing pattern but its q_1 value shifts somewhat to the side of wide scattering angle compared to those for SI61 and $(SI61)_{26}F$ (see Fig. 5c). Table 3 summarized the domain spacings of SI61 diblock arm and $(SI61)_nF$ stars ($n = 7$–77) calculated from SAXS and TEM measurements. It is, however, reasonable that the SAXS pattern of $(SI61)_{77}F$ star is identical to those of SI61 arm and $(SI61)_{26}F$ star within experimental errors. It seems that the formation of the microphase-separated structure of $(SI61)_{77}F$ star depends strongly on the kinetic factor. That is to say, the $(SI61)_{77}F$ star is composed of a large macromolecule ($M_w = 5 \times 10^6$). Then, the $(SI61)_{77}F$ star is difficult to align closely on the interface during the microphase-separation process due to high viscosity. As a result, the lamellae formed showed some kind of curvature.

It is interesting the microphase-separated structures of highly branched $(AB)_n$ stars ($n > 100$) composed of symmetric arms. It can be expected that such stars form a unimolecular micelle even in good solvent and form cubic-like morphology in the bulk. The results obtained will be reported in the near future.

References

[1] Leibler L. Macromolecules 1980;13:1602.
[2] Thomas EL, Alward DB, Kinning DJ, Martin DC, Handlin DL Jr., Fetters LJ. Macromolecules 1986;19:2197.
[3] Alward DB, Kinning DJ, Thomas EL, Fetters LJ. Macromolecules 1986;19:215.
[4] Kinning DJ, Thomas EL, Alward DB, Fetters LJ, Handlin DL Jr., Macromolecules 1986;19:1288.
[5] Herman DS, Kinning DJ, Thomas EL, Fetters LJ. Macromolecules 1987;20:2940.
[6] Anderson DM, Thomas EL. Macromolecules 1988;21:3221.
[7] Thomas EL, Anderson DM, Henkee CS, Hoffman D. Nature 1988;334:598.
[8] Hajduk DA, Harper PE, Gruner SM, Honker CC, Thomas EL, Fetters LJ. Macromolecules 1995;28:2570.
[9] Matsushita Y, Takasu T, Yagi K, Tomioka K, Noda I. Polymer 1994;35:2862.
[10] Ishizu K, Uchida S. Polymer 1994;35:4712.
[11] Ishizu K, Uchida S. J Colloid Interface Sci 1995;175:293.
[12] Ishizu K, Uchida S. J Colloid Interface Sci, to be submitted.
[13] Daoud M, Cotton JP. J Phys (Les Ulis, Fr) 1982;43:531.
[14] Ishizu K, Yukimasa S, Saito R. J Polym Sci, Polym Chem Edn 1993;31:3073.
[15] Ishizu K, Yukimasa S. Polym Commun 1993;34:3753.
[16] Grubisic Z, Rempp P, Benoit H. J Polym Sci B 1967;5:753.
[17] Tsukahara Y, Mizuno K, Segawa A, Yamashita Y. Macromolecules 1989;22:1546.
[18] Grousius P, Gallot Y, Skoulios A. Eur Polym J 1970;6:355.